American Mineralogist, Volume 68, pages 1095–1101, 1983

Programmed cooling experiments in the system MgO–SiO_2: kinetics of a peritectic reaction

R. James Kirkpatrick, Brian H. Reck, Ithamar Z. Pelly,[1] and Lung-Chuan Kuo

Department of Geology
University of Illinois, Urbana, Illinois 61801

Abstract

Programmed cooling experiments with compositions in the system MgO–SiO_2 ranging from 59 wt.% SiO_2 (with olivine on the liquidus) to 63 wt.% SiO_2 (with protoenstatite on the liquidus) cooled at rates of from 0.4 to 25°/min crystallize forsterite but not pyroxene. Because pyroxene does not nucleate, the forsterite plus melt reaction does not take place, allowing forsterite to crystallize metastably at sub-solidus temperatures. A 65.1 wt.% SiO_2 composition (with cristobalite on the liquidus) crystallizes a number of different phases depending on cooling rate and initial superheating. The ease of forsterite nucleation relative to pyroxene offers an explanation for the occurrence of olivine instead of low-Ca pyroxene in the groundmass of tholeiitic basalts and is in agreement with theoretical prediction and previous experiments.

Introduction

Peritectic reactions between coexisting crystals and melt, which in equilibrium produce a new crystalline phase at the expense of the preexisting crystalline phase and melt, are common in magmas of many compositions (see, for instance, the text by Carmichael *et al.*, 1974). The most important peritectic reaction in magmas of basaltic composition is the reaction of magnesium rich olivine and melt to produce low-calcium pyroxene (orthopyroxene or pigeonite). Although a great deal is known about the equilibrium relationships of this reaction in both synthetic and natural compositions, little is known about the kinetics of this or any other peritectic reaction.

The purpose of this paper is to present the results of a set of programmed cooling experiments done with compositions in the system MgO–SiO_2, which is the simplest system exhibiting the olivine plus melt reaction relationship. These experiments indicate that for our experimental configuration, cooling rates of from 0.4 to 25°C/min, and initial superheats of 10°C, pyroxene does not nucleate. Because of this, the forsterite plus melt reaction does not take place, and forsterite crystallizes at sub-solidus temperatures. Indeed, pyroxene never nucleates in any composition on the MgO side of the protoenstatite–cristobalite eutectic, forsterite appearing metastabily instead. At high cooling rates and high initial superheats forsterite even appears for a composition slightly on the silica of the eutectic.

Previous work

Basalts are often classified mineralogically as tholeiitic if they contain crystals of low-calcium pyroxene either as phenocrysts or in the groundmass. Such basalts often contain phenocrysts of olivine, which may be rounded. Many other basalts are orthopyroxene normative but do not contain any low-calcium pyroxene, even in the groundmass. Instead, the low-calcium ferromagnesian phenocryst and groundmass phase is olivine. Most of these basalts without low-calcium pyroxene occur as thin subaerial flows or submarine pillow or sheet flows. Examples include the subaerial flows from Suiko Seamount in the Hawaiian-Emperor chain and most mid-ocean ridge pillow basalts (Bryan, 1972; Kirkpatrick, 1979; Kirkpatrick *et al.*, 1980). Thicker, more slowly cooled bodies and phase equilibrium experiments using similar compositions, however, do produce low-calcium pyroxene (Wright *et al.*, 1976; Walker *et al.*, 1979). The experiments reported here were designed to determine if and under what conditions finite cooling rates can suppress the olivine plus melt reaction in a simple system.

The 1-atmosphere phase equilibrium relationships in the system MgO–SiO_2 have been determined by Bowen and Anderson (1914) and Greig (1927). Figure 1 shows the forsterite to silica portion of the phase diagram and the metastable extensions of some of the phase boundaries. Figure 2 is a blow-up of the central portion of the diagram showing the compositions used in this study. Our undercoolings are reported relative to the liquidus temperatures of this diagram. Examination of the original data indicates that these may be in error by as much as 3 or 4°.

Although there have been no previous kinetic studies along the MgO–SiO_2 join, there have been programmed

[1] Permanent Address: Department of Geology and Mineralogy, Ben-Gurion University, P. O. Box 653, Beer-Sheva, 84120, Israel.

0003–004X/83/1112–1095$02.00

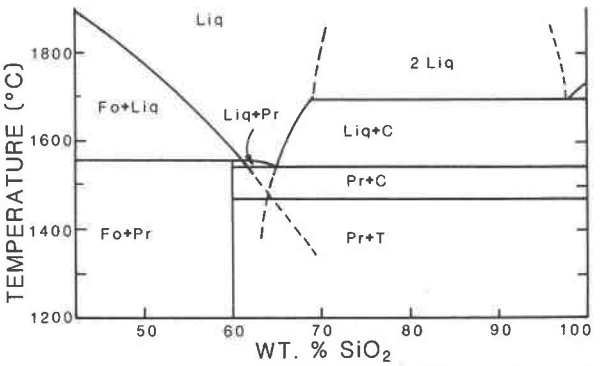

Fig. 1. Phase diagram for the forsterite–silica portion of the system MgO–SiO_2 showing the metastable extensions (dashed) of the forsterite and cristobalite liquidi. After Bowen and Anderson (1914) and Greig (1927).

cooling experiments done with synthetic pyroxene compositions and with basalt compositions which exhibit the reaction relationships.

Programmed experiments with a synthetic melt of diopside composition first crystallize metastable forsterite and then a diopsidic clinopyroxene at under-coolings of between 180° and 240° (Kirkpatrick *et al.*, 1981). The 1-atmosphere equilibrium liquidus phase for this composition is a high-calcium clinopyroxene, and the forsterite only crystallizes when the temperature falls below the metastable forsterite liquidus. One of the objectives of the present study was to determine if metastable olivine nucleation and suppression of pyroxene nucleation also occur in compositions close to a metasilicate composition for which the liquidus phase is olivine rather than a pyroxene.

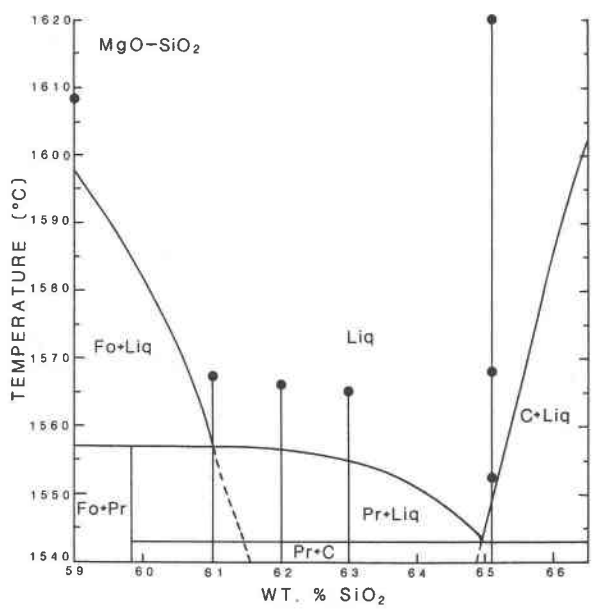

Fig. 2. Central portion of the phase diagram of the system MgO–SiO_2 showing the compositions used in this study and temperatures of initial superheating (dots). After Bowen and Anderson (1914) and Greig (1927).

Programmed cooling experiments with Apollo 15 quartz normative basalts and Luna 24 ferrobasalt, which exhibit the olivine plus melt reaction in equilibrium, do exhibit crystallization of low-calcium pyroxene and dissolution (sometimes complete) of olivine (Grove and Raudsepp, 1978; Grove and Bence, 1979; Lofgren *et al.*, 1979). In some experiments with the Apollo 15 suite at cooling rates greater than 10°/hr., however, euhedral olivines are retained, and olivine and pyroxene apparently crystallize together.

Programmed cooling experiments with the Stannern eucritic meteorite composition co-crystallize olivine and pigeonite at cooling rates of from 5 to 1000°C/hr., even though this composition is very nearly at the peritectic and does not crystallize olivine in equilibrium experiments (Walker *et al.*, 1978). In these experiments the olivine crystallizes at temperatures below its mestable liquidus, and cannot react with the liquid, even though pigeonite is crystallizing.

Experimental procedures

The glass starting materials used in the experiments reported here were prepared from reagent grade MgO and 99.999% pure SiO_2 powder. The glasses were fused three times in a platinum crucible at temperatures about 50° above the liquidus for one hour and ground in an agate mortar and pestle between fusions. Table 1 lists the compositions used and their liquidus temperatures and phases. These compositions range from 59 wt.% SiO_2, which has forsterite on the liquidus, to 65.1% SiO_2, which has cristobalite on the liquidus.

The glass compositions were analyzed using a JEOL model 50A electron microprobe with a Tracor-Northern 4000 automation system, using energy dispersive methods. The beam current was 0.15 nA, the accelerating voltage was 20 kV; and the analytical standard was synthetic forsterite. Atomic number, fluorescence, and

Table 1. Compositions of starting glasses

Nominal composition (wt%)	MgO	41	39	38	37	35
	SiO_2	59	61	62	63	65
Analyzed composition (wt%)	MgO	40.9	38.9	37.8	37.1	34.9[1]
	SiO_2	59.2	60.7	62.2	63.2	65.1
	Total	100.1	99.6	100.0	100.3	100.0

[1]This composition based on the phase diagram of Bowen and Anderson (1914), cristobalite as the liquidus phase, and a liquidus temperature of 1549°C. All others are electron probe analyses (see text).

absorption corrections were made with the program ZAF. Because all the analyses are within the analytical precision of the nominal compositions, we will continue to refer to them by the nominal wt.% SiO_2.

The programmed runs for all compositions except 65.1% SiO_2 were made by placing about 100 mg of glass in a Pt foil boat suspended in the furnace on a Pt wire, heating the sample for 30 minutes at a temperature 10° above the liquidus, and cooling it at a constant rate to the desired quench temperature. Some samples were cooled to a low temperature (about 500°C); others were quenched at relatively small undercoolings. The furnace was a Deltech $MoSi_2$ model 31 with a Eurotherm model 990 SCR controller and a Eurotherm linear temperature programmer. Run products were examined in thin section and by X-ray powder diffraction. Phases were identified by X-ray using the ASTM tables.

Runs with the 65.1% SiO_2 composition were made in the same manner except that they were heated for 30 minutes at temperatures 4°, 20°, and 72° above the liquidus before being cooled to about 500°C and quenched.

Results

Phases present

From the standpoint of the olivine plus melt reaction relationship, the most important result of these experiments is that for cooling rates ranging from 0.4 to 25°C/min the reaction does not take place in any composition examined. In fact, no pyroxene forms in any experiment with any composition on the MgO side of the cristobalite–protoenstatite eutectic. These compositions include those with protoenstatite on the liquidus (which for the equilibrium case end crystallization at the eutectic) and the 59% SiO_2 composition, with olivine on the liquidus (which for the equilibrium case shows the reaction relationship and ends crystallization at the forsterite–protoenstatite peritectic). Very weak tridymite peaks also appear in the X-ray patterns of a few runs with these compositions, although tridymite cannot be identified in thin section. The final assemblage for these compositions, then, is forsterite, glass (which can be identified in thin section), and possibly tridymite.

The behavior of the 65.1% SiO_2 composition (located just on the silica side of the protoenstatite plus cristobalite eutectic) is more complicated. When held at just above the liquidus (4° superheating, by our measurement) for 30 minutes and cooled at a rate of 7°/min it crystallizes protoenstatite and both cristobalite and tridymite. When held 20° above the liquidus for 30 minutes and cooled it crystallizes clinoenstatite (presumably inverted protoenstatite), cristobalite, and tridymite at a cooling rate of 0.4°/min; protoenstatite, cristobalite, and tridymite at cooling rates of 3, 7, and 14°/min; and forsterite and apparently only cristobalite at 25°/min. When cooled from 72° above the liquidus at 7°/min it produces only forsterite and cristobalite. The presence of both cristobalite and tridymite in these runs seems to indicate that crystallization occurs both above and below 1470°C, which is the inversion temperature, although little is known about the metastable crystallization of the silica polymorphs.

Because of our interest in the kinetics of the peritectic reaction, we have looked in more detail at the crystallization sequences of the compositions with 59% SiO_2 (with olivine on the liquidus) and 61% SiO_2 (essentially at the peritectic). These experiments show that forsterite does not begin crystallizing until the temperature is considerably below the liquidus. Figures 3 and 4 show the temperatures of olivine appearance for cooling rates of from 0.4 to 25°C/min for these two compositions. For the 59% SiO_2 composition the highest temperature of olivine appearance is 1533°, an undercooling of 64°. This temperature is 24° below the solidus and well within the forsterite plus protoenstatite stability field. The temperature of first appearance of forsterite may decrease slightly with increasing cooling rate, but certainly no more than a few degrees. There is no rounding of the olivine grains that might indicate dissolution. The runs plotted in Figure 3 contain at the most 10 or 15% crystals, while those cooled to a final temperature of about 500° appear to be almost completely crystallized. The little glass that is left occurs where two dendritic crystals meet. Most of the crystalli-

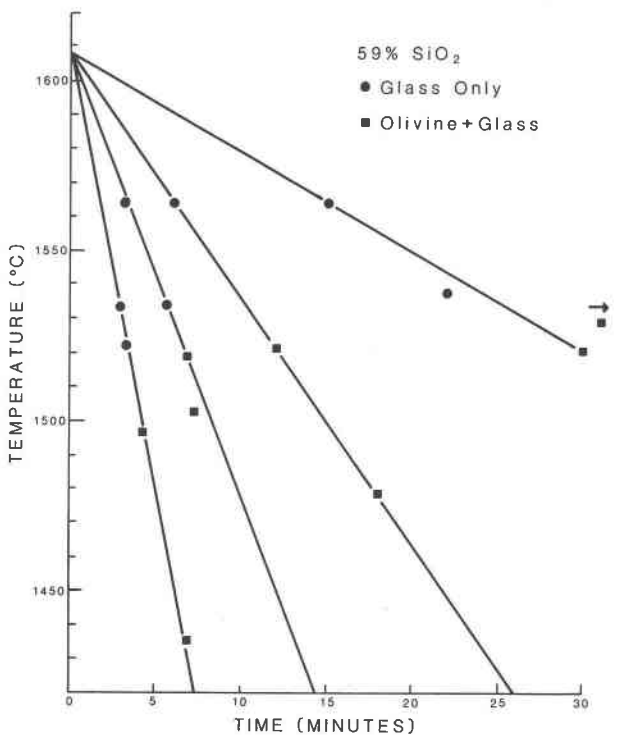

Fig. 3. Time–temperature plot for programmed cooling experiments with the 59% SiO_2 composition. Note that forsterite first appears at an undercooling of about 64°, which is well below the solidus temperature.

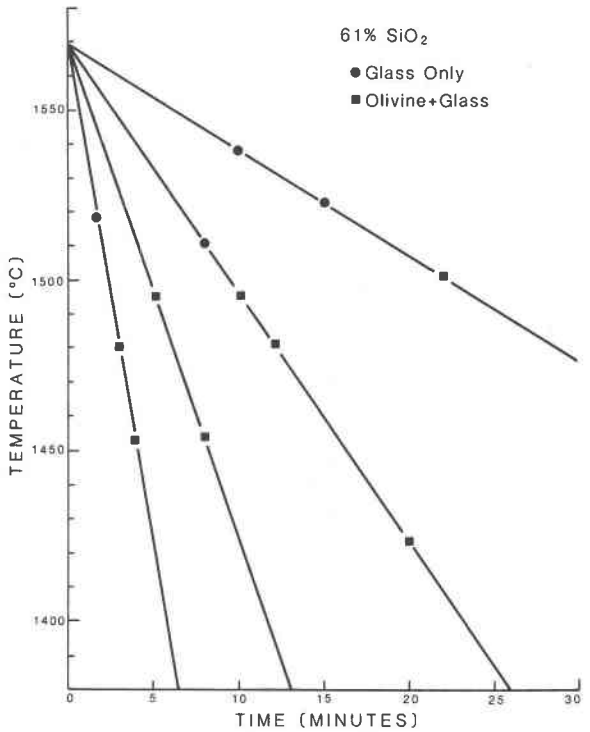

Fig. 4. Time–temperature plot for programmed cooling experiments with the 61% SiO_2 (peritectic) composition. Note that forsterite first appears at an under-cooling of about 55°, which is well below the solidus.

zation, then, must occur at temperatures below those in Figure 3. Tridymite, if it appears, does so at temperatures below the lowest temperature indicated on Figure 3, about 1420°C.

The observed crystallization sequence for the 61% SiO_2 composition is the same as that of the 59% SiO_2 composition. For this composition the forsterite first appears at an undercooling of about 55° (1502°C). This temperature is 41° below the solidus and well within the protoenstatite plus cristobalite field. The temperature of first crystallization does not appear to vary greatly with cooling rate in the range investigated. The runs plotted in Figure 4 contain only a few percent crystals, and most of the crystallization must occur at temperature below 1450°. Tridymite, if it appears, must do so below this temperature.

Crystal morphologies

Olivine-producing runs. The morphologies of the olivine crystals in these experiments are skeletal, dendritic, and spherulitic. The spacing of the individual branches or fibers in the dendrites and spherulites decreases with increasing cooling rate for the same composition and increasing silica content at the same cooling rate. Table 2 summarizes the morphological variations.

For the 59% SiO_2 composition the morphologies are all skeletal or dendritic, and both occur in all samples. Each thin section is composed of fewer than 20 crystal patches, each of which consists of a skeletal olivine crystal surrounded by dendritic olivine that is optically continuous with the skeleton. Figure 5a illustrates this texture. At cooling rates of from 0.4 to 7°/min the skeletons are relatively equant, but at 14°/min they are bladed and similar to barred olivine chrondrules. The spacing of the branches in the dendritic part of the crystals varies from about 5 μm at 0.4°/min to less than 1 micron (not resolvable in thin section) at 14°/min.

For the 61% SiO_2 and 62% SiO_2 compositions the crystals are skeletal with surrounding optically continuous dendrites at the slower cooling rates and feather dendrites at the higher cooling rates. The skeletal crystals with dendrites are similar to those which grow in the 59% SiO_2 composition. The feather spherulites occur in patches composed of feathers that grow radially away from one point. Each feather consists of a central shaft with fibers growing outward at a high angle to it (see Fig. 5b). We have called this morphology spherulitic because each feather is not internally optically continuous, but exhibits the sweeping extinction characteristic of spherulitic non-crystallographic branching (Keith and Padden, 1963). At a cooling rate of 0.4°/min the spacing between the dendrite arms is about 2 μm for the 61% SiO_2 composition and about 1 μm for the 62% SiO_2 composition. At higher cooling rates it is less than 1 μm for both compositions.

The olivines in the 63% SiO_2 composition have a feather spherulite morphology at all cooling rates. At 0.4°/min the fiber spacing is about 1 μm. At higher cooling rates it is less and not resolvable in thin section.

The olivine crystals in the 65.1% SiO_2 composition also occur as feather spherulites with an arm spacing of less than 1 micron. The cristobalite crystals in these runs occur as dendritic crystals up to 1.4 mm long in the run cooled from 72° above the liquidus and as 10 μm equant crystals and 25 μm long dendrites in the run cooled from 20° above the liquidus. In both cases the cristobalite crystals are surrounded by the olivine spherulites. Because the cristobalite dendrites enclosed by each sheaf of spherulites seem to be oriented sub-parallel to each other and in a different orientation from those in other sheaves, it seems likely that the forsterite and cristobalite crystallized simultaneously.

The variation in olivine morphology with cooling rate in these experiments is similar to that seen in programmed cooling experiments with basaltic compositions and with diopside composition melt (Donaldson, 1976; Donaldson *et al.*, 1975; Kirkpatrick *et al.*, 1981). The spacing between the arms or branches is proportional to the ratio of the rate controlling diffusion coefficient in the melt to the growth rate. This ratio decreases with increasing undercooling because the diffusion coefficient decreases exponentially while the growth rate goes up, at least for small to moderate undercoolings. From our data we cannot determine whether the decrease in spacing with increas-

Table 2. Morphologies of olivine crystals for compositions on the MgO side of the protoenstatite–cristobalite eutectic

Cooling Rate (°C/min)	59%	61%	62%	63%
0.4	skeletal surrounded by optically continuous dendritic patches $d \geq 5\,\mu m$	skeletal surrounded by optically continuous dendritic patches $d \geq 1\text{–}2\,\mu m$	skeletal surrounded by optically continuous dendritic patches $d \leq 1\,\mu m$	patches of feather spherulites $d \leq 1\,\mu m$
3	skeletal surrounded by optically continuous dendritic patches	No thin section	optically continuous dendritic patches + a few spherulitic patches	patches of feather spherulites
7	skeletal surrounded by optically continuous dendritic patches	skeletal with a few dendritic patches, mostly patches of feather spherulites	patches of dendrites and feather spherulites	patches of feather spherulites
14	bladed skeletal $d < 1\,\mu m$	feather spherulites	No thin section	No thin section
25	No thin section	feather spherulites $d \ll 1\,\mu m$	patches of feather spherulites $d \ll 1\,\mu m$	patches of feather spherulites $d \ll 1\,\mu m$

d is the spacing between the axies of dendrite arms or spherulite fibers.

ing SiO_2 content at constant cooling rate is due to crystallization at larger undercoolings or to a decrease in the diffusion coefficient to growth rate ratio.

Pyroxene-producing runs. The protoenstatite in the experiments with the 65.1% SiO_2 composition cooled from just above the liquidus (4° superheat, by our measurement) at 7°/min occurs as equant patches of dendritic grains. At low magnification these crystals appear to be normal complete crystals, and it is only at high magnification that the dendritic pattern can be seen. Apparently they grew as dendrites and later filled in between the arms. The tridymite and cristobalite occur as faceted equant crystals 10 to 20 μm across. They are poikilitically enclosed by the pyroxene and appear to have crystallized first. Figure 5c illustrates this texture.

The clinoenstatite in the runs with the 65.1% SiO_2 composition cooled from 20° above the liquidus at 0.4°/min occurs as dendritic patches similar to those in the runs cooled from 4° above the liquidus, while the protoenstatite in the faster runs cooled from 20° above the liquidus occurs as feather spherulites. The tridymite and cristobalite in these runs occur as dendritic crystals up to 0.3 mm long and as equant crystals up to 25 μm across (Fig. 5d). The silica phases are surrounded by the pyroxene and appear to have crystallized first.

Discussion

Crystallization processes and nucleation

Our primary objective in this study is to determine in the simplest possible system if and how the olivine plus liquid reaction relationship actually takes place under continuous cooling conditions. The results for the 59% SiO_2 composition, which is the only composition that

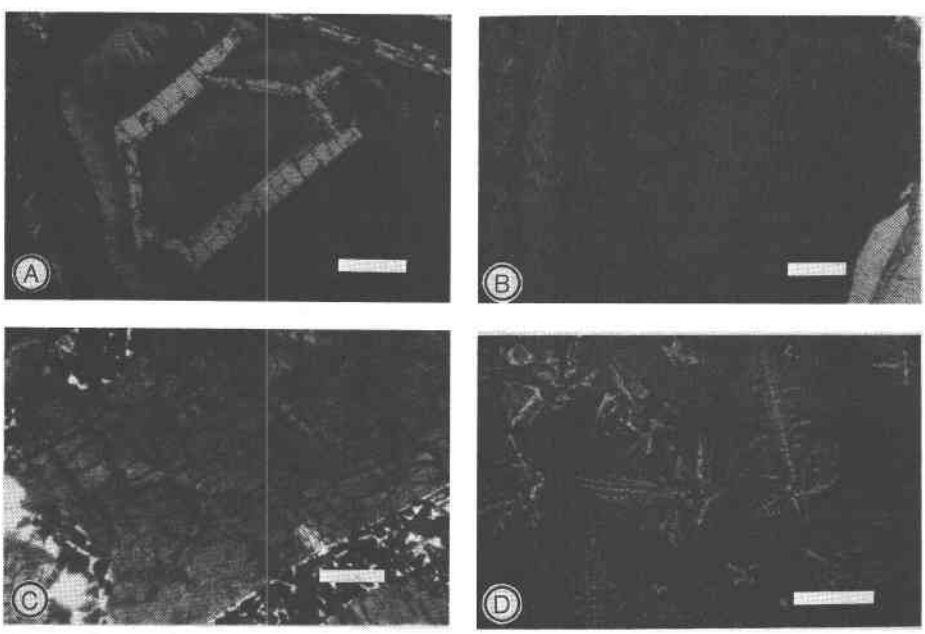

Fig. 5. Photomicrographs of thin sections of programmed experiments. (a) 59% SiO_2, 3°/min, skeletal olivine surrounded by optically continuous dendritic olivine. Scale bar is 0.2 min. (b) 61% SiO_2, 14° min. Feather spherulitic olivine. Scale bar is 0.2 mm. (c) 65.1% SiO_2, 7°/min. Protoenstatite with small, poikilitically enclosed grains of a silica phase. Scale bar is 0.2 mm. (d) 65.1% SiO_2, 14°/min. Equant and dendritic cristobalite and tridymite surrounded by protoenstatite. Scale bar is 0.1 mm.

should show the reaction in equilibrium, indicate that under our experimental conditions this reaction does not take place. Instead, crystallization takes place by nucleation and growth of first olivine and then pyroxene. Dissolution of olivine does not occur. This crystallization starts at temperatures well below the solidus, which for the 59% SiO_2 composition is also the temperature at which the olivine plus liquid reaction should take place if equilibrium were to prevail. The reason that crystallization occurs in this way is that nucleation of both phases does not occur until considerable deviation from equilibrium is reached.

The delay in nucleation and the crystallization of olivine before pyroxene at large undercoolings continues to more silica-rich compositions, which have pyroxene on the liquidus. For these compositions crystallization starts out not only below the solidus temperature but also below the metastable extension of the olivine liquidus.

The reason for this behavior seems to be that nucleation in these experiments is dominated by transient behavior. According to classical nucleation theory (Kaschiev, 1969) if a melt is cooled from above to below its liquidus, it takes a finite length of time for the small, crystal-like clusters of atoms that exist in the melt above the liquidus to grow to the size of the critical nucleus. This critical size decreases with increasing undercooling. Under conditions of continuous cooling crystal-like clusters are growing as time proceeds and temperature falls. Simultaneously the size of the critical nucleus is decreasing. Nucleation occurs at the time and temperature when the size of the largest cluster becomes the same as the critical size. Because the growth of sub-critical clusters involves random attachment and detachment of atoms or molecular groups, the temperature at which nucleation occurs is not necessarily exactly the same for different experiments run at the same cooling rate under exactly the same conditions.

This metastable nucleation of olivine appears to be in agreement with a theory of transient nucleation in silicate melts developed by Kirkpatrick (1983). This theory predicts that if two crystalline phases are stable relative to the melt, the less polymerized one will nucleate first if structural units at least as depolymerized as itself are available in the melt. This seems to be true for all compositions used here.

The 65.1% SiO_2 composition, which is the most silica-rich composition we could investigate and which nucleates olivine metastabily when cooled from 72° above the liquidus, has a non-bridging oxygen to tetrahedral cation ratio of about 1.6 (Mysen *et al.*, 1980). For this ratio Mysen *et al.* predict that the melt structure should consist of silica monomers, chains, and sheet-like units. All the less silica-rich compositions should also contain silica monomer units. According to this theory of transient nucleation the presence of silica monomers in the melt should allow more rapid transient nucleation of crystals with an isolated tetrahedra structure (*i.e.*, olivine) than those with more polymerized structure (pyroxene). This is exactly what is observed.

Comparison with mineralogy and texture of basalts

The results of these experiments offer a useful model for understanding why olivine replaces or occurs with low-calcium pyroxene in the groundmass of so many tholeiitic basalts. It seems likely that pyroxene is as difficult to nucleate in nature as it is in our experiments. This allows olivine to crystallize along or below its metastable liquidus. Low-calcium pyroxene may or may not nucleate. If it does, olivine, low-calcium pyroxene, and high-calcium pyroxene all occur in the groundmass. If it does not, olivine and high-calcium pyroxene occur. Both situations are observed in Hawaiian-Emperor chain basalts (Kirkpatrick *et al.*, 1980). Low-calcium pyroxene is extremely rare in mid-ocean ridge basalts (Kirkpatrick, 1979).

There are many limitations, besides bulk composition, on even the qualitative application of our experimental results to natural situations. One of these is that many tholeiitic basalts are erupted with faceted olivine phenocrysts, which indicate that olivine is already crystallizing and that there are already many olivine-like clusters with sizes near that of the critical nucleus. In this case the groundmass olivine might begin crystallizing at smaller undercoolings than if the lava were significantly superheated. If there are no phenocrysts of low-calcium pyroxene, the lava is likely to be superheated with respect to this phase, and nucleation would be dominated by transient effects, as it is in the experiments.

It should be pointed out, however, that if the cooling rate is fast enough, olivine nucleation can be suppressed even if faceted olivine phenocrysts are present. This occurs in glassy chill margin of many submarine and subaerial lava flows, where no post-eruption crystals are present.

Whether olivine can occur metastably instead of low-calcium pyroxene in plutonic rocks is not known, although Walker *et al.* (1979) have shown how magma mixing can produce significant undercoolings even in slowly cooled bodies.

Another important difference between our experiments and nature is the mode of nucleation. In the experiments nucleation is probably occurring heterogeneously, quite possibly on the walls of the platinum capsules, although this is difficult to prove. In nature nucleation probably also occurs heterogeneously (Kirkpatrick, 1979) but on silicate material (either phenocrysts or groundmass crystals, reincorporated chilled crust, or other incorporated solid material). How significant this limitation is on the usefulness of the experimental data is difficult to determine. The lack of low-calcium pyroxene and the occurrence of olivine in so many tholeiitic basalts, however, would seem to indicate that our results are applicable.

Additional support for the model comes from the

morphologies of the olivine crystals in the experiments and in lava flows. Skeletal olivine crystals surrounded by optically continuous dendritic olivine that grew from the skeleton are common in both the experiments and the margins of mid-ocean ridge pillow basalt flows (Kirkpatrick, 1979). This change in morphology as the crystal grows implies a continual increase in the undercooling as crystallization proceeds. The dendritic morphology implies tens to perhaps a few hundred degrees undercooling and no dissolution of the olivine. Feather spherulites of olivine similar to those in our experiments are also common in many submarine pillow basalts (Bryan, 1972).

Acknowledgments

This work was supported by NSF Grants EAR 79-03923 and EAR 82-07260. Reviews by Drs. Philip Fenn and Eric Dowty greatly improved the original version of the paper.

References

Bowen, N. L. and Anderson, O. (1914) The binary system MgO–SiO_2. American Journal of Science, 187, 4881.

Bryan, W. B. (1972) Morphology of crystals in submarine basalts. Journal of Geophysical Research, 77, 5812–5819.

Carmichael, I. S. E., Turner, F. J., and Verhoogen, J. (1974) Igneous Petrology. McGraw Hill, New York.

Donaldson, C. H. (1976) An experimental investigation of olivine morphology. Contributions to Mineralogy and Petrology, 57, 187–213.

Donaldson, C. H., Usselman, T. M., Williams, R. J. and Lofgren, G. E. (1975) Experimental modeling of the cooling history of Apollo 12 olivine basalt. Proceedings of the Lunar Science Conference 6th, 843–869.

Greig, J. W. (1927) Immiscibility in silicate melts. American Journal of Science, 213, 1–44 and 137–154.

Grove, T. L. and Bence, A. E. (1977) Experimental study of pyroxene-liquid interaction in quartz-normative basalt 15597. Proceedings of the Lunar Science Conference 8th, 1549–1579.

Grove, T. L. and Raudseep, M. (1978) Effects of kinetics on the crystallization of quartz normative basalt 15587: an experimental study. Proceedings of the Lunar Science Conference 9th, 585–599.

Kaschiev, D. (1969) Solution of the non-steady state problem in nucleation kinetics. Surface Science, 14, 209–270.

Keith, H. D. and Padden, F. J. (1963) A phenomenological theory of spherulitic crystallization. Journal of Applied Physics, 34, 2409–2421.

Kirkpatrick, R. J. (1979) Processes of crystallization in pillow basalt, Hole 396B, DSDP Leg 46. Initial Reports of the Deep Sea Drilling Project, 46, 271–282.

Kirkpatrick, R. J. (1983) Theory of nucleation in silicate melts. American Mineralogist, 68, 66–77.

Kirkpatrick, R. J., Clague, D. A., and Freisen, W. A. (1980) Petrology and geochemistry of volcanic rocks, DSDP Leg 55, Emperor seamount chain. Initial Reports of the Deep-Sea Drilling Project, 55, 509–557.

Kirkpatrick, R. J., Kuo, L. C., and Melchior, J. (1981) Crystal growth in incongruently melting compositions: programmed cooling experiments with diopside. American Mineralogist, 66, 223–241.

Lofgren, G. E., Grove T. L., Brown, R. W., and Smith, D. P. (1979) Comparison of dynamic crystallization techniques on Apollo 15 quartz normative basalts. Proceedings of the Lunar Science Conference 10th, 423–438.

Mysen, B. O., Virgo, D., and Scarfe, C. M. (1980) Relations between the anionic structure and viscosity of silicate melts—a Raman spectroscopic study. American Mineralogy, 65, 690–710.

Walker, D., Powell, M. A., Lofgren, G. E., and Hays, J. F. (1978) Dynamic crystallization of a eucrite basalt. Proceedings of the Lunar Science Conference 9th, 1369–1391.

Walker, D., Shibata, T. and DeLong, S. E. (1979) Abyssal tholeiites from the oceanographer fracture zone II. Phase equilibria and mixing. Contributions to Mineralogy and Petrology, 70, 111–125.

Wright, T. L., Peck, D. L., and Shaw, H. R. (1976) Kilauea lava likes: natural laboratories for study of cooling, crystallization, and differentiation of basaltic magma. In G. H. Sutton *et al.*, Eds., The Geophysics of the Pacific Ocean Basin and its Margin, Geophysical Monograph 19, p. 375–390. American Geophysical Union, Washington D.C.

Manuscript received, June 18, 1982;
accepted for publication, May 9, 1983.